

Journal of Biomedical Optics

SPIEDigitalLibrary.org/jbo

Deep-penetration photoacoustic array imaging of calcifications

Tsai-Chu Hsiao
Yao-Yu Cheng
Wan-Ting Tein
Shih-Bin Luo
De-Yi Chiou
Ren-Jei Chung
Meng-Lin Li



SPIE

Deep-penetration photoacoustic array imaging of calcifications

Tsai-Chu Hsiao,^{a*} Yao-Yu Cheng,^{b*} Wan-Ting Tein,^c Shih-Bin Luo,^c De-Yi Chiou,^c Ren-Jei Chung,^d and Meng-Lin Li^{a,b}

^aNational Tsing Hua University, Institute of Photonics Technologies, Hsinchu 30013, Taiwan

^bNational Tsing Hua University, Department of Electrical Engineering, Hsinchu 30013, Taiwan

^cIndustrial Technology Research Institute, Electronics and Optoelectronics Research Laboratories, Hsinchu 31040, Taiwan

^dNational Taipei University of Technology, Graduate Institute of Biotechnology, Taipei 106, Taiwan

Abstract. Calcifications are one of the most important indicators for early breast cancer detection. We explore the feasibility of deep-penetration photoacoustic (PA) imaging of calcifications based on a medical ultrasound array imaging platform. Intralipid and chicken breast phantoms embedded with different-sized hydroxyapatite (HA) particles, which are the major components of calcifications, were imaged to verify the equipment's capability and penetration depth for the visualization of calcifications. An optimal near-infrared excitation wavelength was selected to maximize PA signals of HAs, resulting in a better HA signal-to-blood ratio. We demonstrated that PA imaging is capable of visualizing 0.5-mm HA particles at a depth of 3 cm in chicken breast phantoms. The noise-equivalent penetration depth of the system for visualizing 0.5-mm HA particles in the human breast was estimated to be about 2.9 to 3.5 cm, which is clinically relevant as calcifications are usually found at a depth of 0.6 to 3.0 cm. Moreover, the feasibility of differentiating HA from blood by the PA spectroscopic technique was presented and the mechanism of the HA signal generation was discussed. The results show that PA imaging is a promising technique for real-time visualization of breast calcifications. © 2013 Society of Photo-Optical Instrumentation Engineers (SPIE) [DOI: 10.1117/1.JBO.18.6.066002]

Keywords: photoacoustic imaging; breast calcifications; breast cancer.

Paper 12823RR received Dec. 28, 2012; revised manuscript received May 8, 2013; accepted for publication May 10, 2013; published online Jun. 3, 2013.

1 Introduction

In x-ray mammography, the size, number, and clustering of microcalcifications are important features for grading the suspicious lesions based on BI-RADS classification scale.¹ Currently, x-ray mammography is the standard for breast cancer screening; however, its use exposes patients to the carcinogenic risks of ionizing radiation. Ultrasound is recommended as the appropriate modality for the evaluation of palpable breast masses. One challenge is the difficulty of imaging calcifications smaller than 1 mm due to poor contrast resulting from inherent speckle noise.² Therefore, a new modality that combines the calcification imaging capabilities of x-ray mammography and the non-ionization feature of ultrasound is warranted. Photoacoustic (PA) imaging is an emerging imaging modality capable of real-time, nonradioactive, and high-resolution optical imaging of tissues with deep penetration. Among the various PA imaging techniques investigated to date, near-infrared (NIR) PA imaging of angiogenesis is of particular interest for noninvasive breast diagnosis because of the high absorption contrast between hemoglobin and other breast tissues.^{3,4} Using a custom-made 10-MHz photoacoustic microscopy (PAM) setup, we have demonstrated the feasibility of using PA imaging for high-contrast visualization of calcifications, which may potentially be utilized as an auxiliary tool to conventional breast ultrasound and x-ray mammography.⁵ At a depth of 2 mm, the PA

signal of 0.5 mm granulated hydroxyapatite (HA)—a major chemical composition of breast calcifications associated with malignant and benign lesions⁶—rivals that of blood, the dominant optical absorber, at a wavelength of 750 nm. Recently, Kang et al. have also validated the use of PA imaging of calcifications within core-biopsied breast tissue of 3.5 mm thickness by shining a laser directly onto the sample.⁷ The calcification imaging systems presented in these studies show limited penetration depth and are not sufficient for diagnosis and biopsy guidance. Although Song and Wang have demonstrated that a PAM-like setup, using a 5-MHz single-element transducer with long focal depth, can provide penetration up to 38 mm in a chicken breast phantom for imaging of blood content,⁸ real-time imaging capability and extended depth of focus with dynamic receive focusing technique are not feasible. Both features are required for real-time diagnosis and biopsy guidance, which can be provided with an array imaging system.

Therefore, in this study, we investigate the feasibility of deep-penetration PA imaging based on a medical ultrasound array imaging platform to visualize calcifications. First, an optimal excitation wavelength was selected to maximize the PA signals from HA particles and to optimize the ratio of HA to blood signal, in order to reduce the interference of blood signals for calcification imaging. Intralipid and chicken breast phantoms embedded with different-sized HA particles were imaged to verify the achievable imaging depth of the custom-built system for the visualization of calcifications. We further showed that the PA spectroscopic technique is capable of differentiating HAs from blood. Finally, the noise-equivalent penetration depth of

*Tsai-Chu Hsiao and Yao-Yu Cheng have contributed equally to this work.

Address all correspondence to: Meng-Lin Li, National Tsing Hua University, Department of Electrical Engineering, No. 101, Section 2, Kuang-Fu Rd., Hsinchu, Taiwan 30013. Tel: +886-3-516-2179; Fax: +886-3-571-5971; Email: mlli@ee.nthu.edu.tw

the system for visualizing HAs in human breast is further calculated according to the PA signal intensity obtained in phantom studies and the acoustic and optical attenuation coefficients of human breast from the literature.

2 Materials and Methods

2.1 Measurement of PA Spectrum of HA Particles

To select an optimal excitation wavelength of HAs for the following PA array imaging experiments, PA signals from HA particles at different optical wavelengths (i.e., PA spectrum of HA particles) were measured with a 5-MHz dark-field backward-mode confocal PAM setup.⁵ The PAM setup was equipped with a photodiode, while the array imaging setup used for the following imaging experiments did not have the photodiode channel. The photodiode signals could be used to compensate for PA signal variations caused by laser-energy fluctuations and differences in laser output at different wavelengths. For a spectroscopic study, such compensation is necessary; therefore, PAM was utilized here instead of the array setup. An optical parametric oscillator (Surlite OPO Plus, Continuum, USA) pumped by a frequency-doubled Q-switched Nd:YAG laser (Surlite II-10, Continuum, USA) was employed to provide laser pulses with a pulse width of ~ 4 ns and a pulse repetition rate of 10 Hz. Laser energy was delivered by a 1-mm multimode fiber. The fiber tip was coaxially positioned with a convex lens, an axicon, a plexiglass mirror, and a 5-MHz focused ultrasonic transducer (V310-SM, Olympus, USA) on an optical bench, which created dark-field illumination and made the light confocal with the ultrasonic transducer. The optical bench was fixed on a three-dimensional precision translation stage, upon which the x and y axes were motorized and the z axis could be manually adjusted with a micrometer. The PA signals received by the 5-MHz transducer were preamplified by a low-noise amplifier (AU-3A-0110, Miteq, USA), cascaded to an ultrasonic pulser/receiver (5073 PR, Olympus, USA), low-pass filtered, digitized by a PC-based 14-bit analog-to-digital card (CompuScope 14200, GaGe, USA), sampled at 200 MHz, and then recorded onto a PC. Before any further signal processing, signals from a photodiode (DET36A/M, Thorlabs, USA) were used to compensate for PA signal variations caused by laser-energy instability and differences in laser output at different wavelengths.

An NIR window between 670 and 850 nm was selected due to the relatively lower optical absorption of hemoglobin, lipids, and water in this window, and thus deeper penetration could be potentially achieved.³ The granulated HA particles were prepared with commercially available HA powder (Plasma Biotol Ltd., Tideswell, UK). The HA powder was sintered at 900 to 1000°C for 2 to 4 h in a dry air atmosphere to form polycrystalline calcification particles. The typical size of breast calcifications is between 0.3 and 1.0 mm.⁹ Therefore, six granulated HA particles with the size of about 0.5 to 1 mm were used. The particles were fixed on a clear porcine gel phantom during the measurement by a thin layer of porcine gel, and 1000 measurements were taken at each wavelength for each particle in order to improve the signal-to-noise ratio (SNR) and further reduce the effects of laser energy fluctuation.

2.2 Experimental Setup of PA Array Imaging

Based on a medical ultrasound array imaging platform, a PA array imaging system was built to verify the achievable imaging

depth for visualizing calcifications. The array imaging system could provide the real-time imaging capability and potentially extend the depth of focus with dynamic receive focusing technique. In addition, it was inherently compatible with clinical ultrasound, thus enabling PA/ultrasound dual modal imaging. The PA array imaging system was used here for deep tissue imaging of calcifications. The experimental setup was as illustrated in Fig. 1. The laser utilized here was the same as the one used for the PA spectrum measurements. A 5-MHz and 128-element medical ultrasound linear array with a fractional bandwidth of 71% (AT5L40B, BroadSound Corporation, Taiwan) was used for PA signal detection. The -6 -dB axial and lateral resolutions of this PA array imaging system were 0.54 and 0.35 mm at the depth of 3 cm, respectively. The detected PA signals were acquired and digitized with a PC-based ultrasound array data acquisition system—Verasonics V-1 (Verasonics Inc., Redmond, Washington). Image reconstruction was done on the control PC where a delay-and-sum beam-forming algorithm was employed. To improve image contrast, coherence factor weighting¹⁰ was also applied. Side-way illumination, instead of the dark-field geometry used in PAM, was adopted here because it was easier to implement, providing a relatively uniform optical fluence over the imaging plane of the array transducer. Two types of phantoms—intralipid and chicken breast phantoms—were used for this study. The intralipid phantom was prepared using gelatin (gelatin, G2500-1KG, Sigma-Aldrich, St. Louis, Missouri) as the matrix with the addition of 1% of intralipid (Lipovenoes 20%) as an optical scatterer. A double-integrating-sphere setup along with the inverse adding doubling algorithm was used to determine the optical absorption coefficient (μ_a) and reduced optical scattering coefficient (μ_s) of the phantoms.¹¹ The study objects (e.g., HA particles and blood-loaded tubes) were positioned so that their optical and acoustic depths were both ~ 3 cm in the phantoms, as illustrated in Fig. 1. Note that in the following phantom experiments, signal averaging of 20 times was performed to improve the SNR.

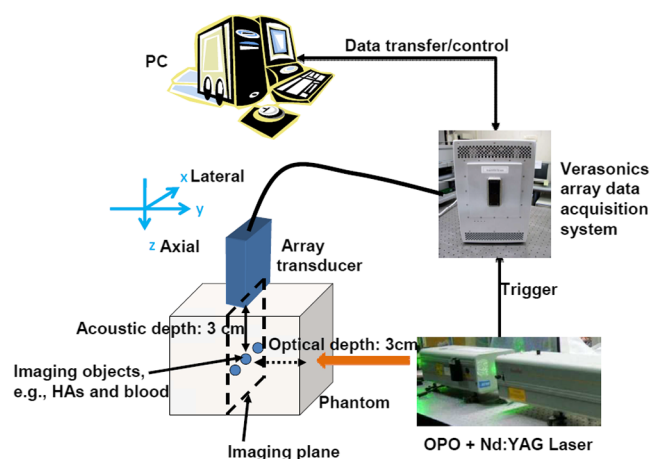


Fig. 1 Illustration of experimental setup of PA array imaging. The optical depth indicated by the horizontal double-headed dotted line represents the distance from the laser illumination surface to the imaging plane; the acoustic depth indicated by the vertical double-headed solid line is the distance from the transducer surface to the imaging objects in the imaging plane. The dashed parallelogram illustrates the imaging plane beneath the array transducer.

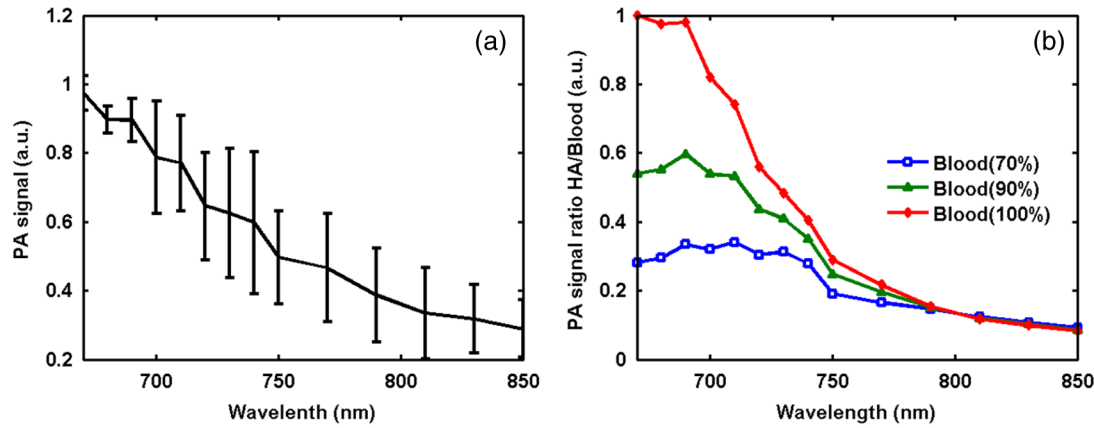


Fig. 2 (a) Amplitude of measured PA signals as a function of wavelength from six HA particles with sizes ranging from 0.5 to 1 mm. The error bar is the standard deviation of the six measurements of the HA particles. (b) Calculated PA signal ratios of HA to blood with different SO_2 between 670 and 850 nm. a.u., arbitrary unit.

3 Results and Discussions

Figure 2(a) shows the normalized PA signals measured from six granulated HA particles at excitation wavelengths ranging from 670 to 850 nm. The PA signal of the HA particles showed a tendency to decrease with a longer optical wavelength, which is substantially consistent with the reported optical absorption spectrum of HA.^{12,13} The PA spectrum of HA particles was further compared with that of blood—a dominant optical absorber in human breast tissue. Figure 2(b) shows the calculated PA signal ratios of HA to blood with different oxygen saturation (SO_2) as a function of wavelength. This figure was plotted based on the compiled molar extinction spectral data of oxy- and deoxy-hemoglobin provided by Oregon Medical Laser Center (<http://omlc.ogi.edu>), an assumed typical hemoglobin concentration for whole blood of 150 g Hb/liter, and the proportionality of PA signals from blood to absorption coefficients of blood with different SO_2 .¹⁴ Only blood with SO_2 ranging from 70 to 100% was considered here because the average SO_2 of arterial and venous blood is >95% and 70 to 75%, respectively. From Fig. 2(a) and 2(b), we ascertained that around 700 nm, stronger PA signals of HA particles and a higher signal ratio of HA to blood were obtained. In addition, our laser output was more stable with higher energy at 700 nm. Therefore,

the wavelength of 700 nm was selected as the excitation wavelength for the array imaging experiments.

An ultrasound speckle-generating intralipid phantom with a blood-loaded tube and different-sized HA particle embedded was imaged first. The measured μ_a and μ_s' of the intralipid phantom were 0.06 and 5.09 cm^{-1} at 700 nm, respectively, which are close to the reported data on postmenopausal breast tissues at 700 nm.¹⁵ A blood-loaded tube with a 0.25-mm inner diameter and HA particles with about 1.0 and 0.5 mm size were placed in a row within the imaging plane, as illustrated in Fig. 1. The depths of all the HA particles from the transducer surface (i.e., acoustic depth in Fig. 1) and from the laser illumination surface (i.e., optical depth in Fig. 1) were approximately 3.0 cm, respectively. The laser exposure on the sample surface was about 18 mJ/cm^2 at 700 nm, which was well within the American National Standards Institute safety limit of 20 mJ/cm^2 . Figure 3(a) depicts the ultrasound B-mode image used as a reference to locate the imaging objects. Figure 3(b) represents the PA B-mode image acquired at a wavelength of 700 nm, revealing the high contrast feature of PA imaging compared with pulse-echo ultrasound. From left to right are cross-sections of the blood-loaded tube and 1.0- and 0.5-mm HA particles positioned at the depth of ~ 3 cm, respectively. The estimated SNRs for the blood-loaded tube, the 1.0-mm

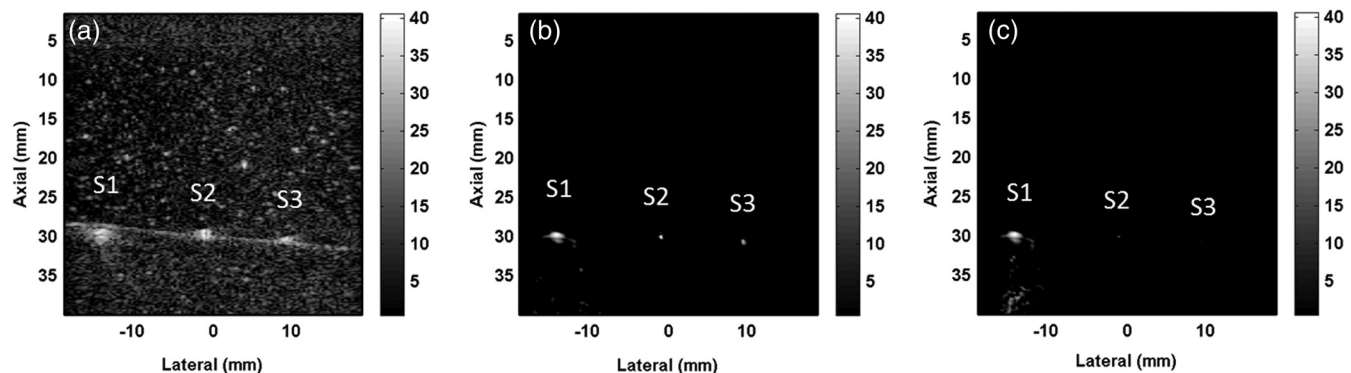


Fig. 3 Ultrasound and PA B-mode images of the cross-sectional blood-loaded tube, 1.0-mm HA particle, and 0.5-mm HA particle, which are all displayed on a 40-dB dynamic range. (a) Ultrasound B-mode image, (b) PA B-mode image acquired at the wavelength of 700 nm, (c) PA B-mode image acquired at the wavelength of 800 nm. S1, blood-loaded tube; S2, 1.0-mm HA particle; S3, 0.5-mm HA particle. Note that in (b) and (c), the PA signals were normalized by the peak intensity of S1.

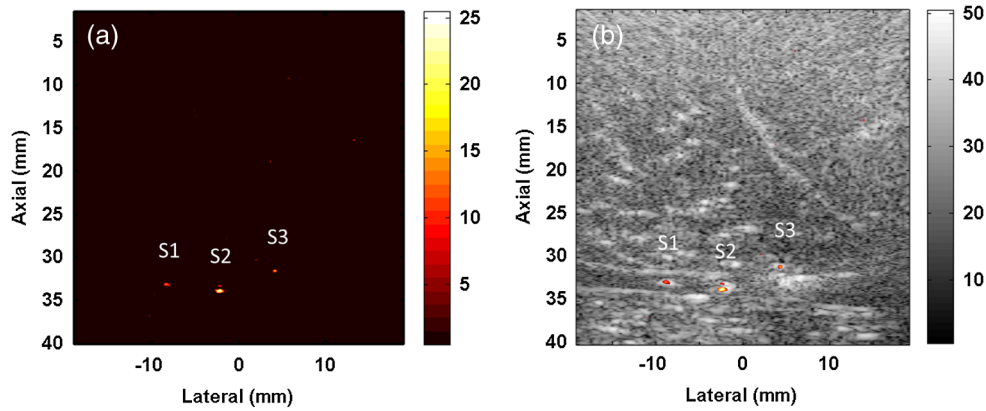


Fig. 4 PA and PA/ultrasound coregistered B-mode images of a chicken breast phantom with HA particles embedded. (a) PA B-mode images acquired at the wavelength of 700 nm and displayed over a 25-dB dynamic range. (b) PA/ultrasound coregistered B-mode image, where the ultrasound image is displayed over a 50-dB dynamic range. S1, 0.5-mm HA particle; S2, 1.0-mm HA particle; S3, 0.5-mm HA particle.

HA particle, and the 0.5-mm HA particle were 43.2, 35.7, and 29.6 dB, respectively, indicating that deeper penetration can be achieved. The SNR was defined as the peak of the PA signals obtained from the objects divided by the root mean square of the background signals. Figure 3(c) illustrates the PA B-mode image acquired at a wavelength of 800 nm. In Fig. 3(b) and 3(c), the PA signals were normalized by the peak signal intensities of the blood-loaded tube at 700 and 800 nm, respectively. In addition, the averaged laser exposure at 700 and 800 nm was carefully checked and kept constant during the experiments due to the lack of a photodiode channel in the array imaging system for compensation of the PA signal variation caused by laser energy fluctuation. The signals of HA particles decreased relative to those in Fig. 3(b). This trend follows the spectral curves portrayed in Fig. 2(b), which were also normalized to the blood signals. These results indicated the feasibility of differentiating the HA signals from blood by the PA spectroscopic technique.

In addition, a chicken breast phantom experiment was performed to further evaluate the achievable imaging depth of the system for visualizing calcifications in real tissues. The measured μ_a and μ_s' of the chicken breast phantom were 0.25 and 3.26 cm^{-1} , respectively, at 700 nm. Three HA particles were embedded in a row within the imaging plane. Figure 4(a) shows the PA B-mode image of the chicken breast phantom. The HA particles of all sizes could be identified due to the high contrast and speckle-free PA image. From left to right, HA particle sizes were 0.5, 1.0, and 0.5 mm, respectively. The estimated SNRs of the particles from left to right were 14.1, 19.6, and 15.5 dB, respectively. Compared with those in the intralipid phantom, the lower SNRs of HA particles in the chicken breast phantom were caused by the higher effective optical attenuation coefficient of the chicken breast phantom. Figure 4(b) illustrates the ultrasound B-mode image coregistered with the PA image in Fig. 4(a). The threshold used for the coregistration was 25 dB. In the ultrasound image, HA particles were barely identified because of speckle noises and hyperechoic spots from chicken breast tissues. The coregistration of the PA and ultrasound images was helpful in localizing the HA particles within a structural ultrasound background image.

The maximum achievable depth for imaging HAs in human breast is derived as follows. From the μ_a and μ_s' of the experimental chicken breast, its calculated optical attenuation at 700 nm is 7.0 dB/cm and its reported acoustic attenuation is about 2.0 dB/cm at 5 MHz, which is the center frequency of

the used array transducer.¹⁶ The two-way PA attenuation of the chicken breast is the summation of the optical and acoustic attenuation, which is 9.0 dB/cm in this case. Without attenuation, the SNR of the 0.5-mm HA particle would have been 41 dB. Similarly, according to the acoustic attenuation [i.e., 8.4 dB/cm at 5 MHz (Ref. 17)] and the reported μ_a and μ_s' of the human breast,¹¹ the resultant two-way PA attenuation is 14.0 dB/cm for premenopausal breast and 11.7 dB/cm for postmenopausal breast. Therefore, the calculated noise-equivalent penetration depth for 0.5-mm HA is about 2.9 cm in premenopausal breast and about 3.5 cm in a postmenopausal breast, which is suitable for clinical applications because breast calcifications are located mostly at the depth of 0.6 to 3.0 cm.¹⁸ As for the mechanism of the HA signal generation, the magnitude of the HA signal is contributed to from both μ_a and Grüneisen coefficient.¹⁹ It is found that the μ_a of HA [i.e., 0.75 cm^{-1} (Ref. 9)] is smaller than that of whole blood (i.e., $\sim 3.97 \text{ cm}^{-1}$) by about five times at the wavelength of 700 nm, while the Grüneisen coefficients of whole blood and dental enamel, in which at least 96% is HA, are about 0.25 and 1.4, respectively.^{13,15} Presumably, the Grüneisen coefficient contributes greatly to the HA signal.

4 Conclusions

In summary, we have successfully demonstrated that by using a medical ultrasound array imaging platform at an optimal wavelength of 700 nm, the HA calcification particles of size 0.5 mm can be visualized at a depth of 3 cm in a chicken breast phantom with an SNR of 14.1 dB. Prior data from the literature suggests that with our 5-MHz PA array imaging system, we should expect a penetration depth of about 2.9 to 3.5 cm for visualization of calcifications in human breast. This depth coverage is clinically relevant as most calcifications occur at this depth. It should be noted that this study does not exclude the value of PA imaging of breast tumor vascularization—also an important feature of breast cancer. PA visualization of microcalcifications without interference from other absorbers, such as blood, could provide additional value to conventional ultrasound- and also angiogenesis-contrast-based PA breast imaging. We demonstrated the feasibility that HA can be differentiated from blood by using the PA spectroscopic technique. The penetration depth and specificity can be further improved by introducing NIR fluorescent optical contrast agents targeting HA.²⁰ In addition, our results suggest that PA/ultrasound dual modal imaging may

enhance the identification of anatomical locations of calcifications, which complements x-ray mammography typically for dense breast²¹ and breast ultrasound. Overall, PA imaging coregistered with breast ultrasound shows great promise as a real-time diagnosis and biopsy guidance tool for visualization of breast calcifications.

Acknowledgments

We would like to acknowledge funding support from the Electronics and Optoelectronics Research Laboratories, Industrial Technology Research Institute, Taiwan (A351AA5110, A101W32H00, and B101W32K00), the National Science Council, Taiwan (NSC 100-2221-E-007-010-MY2), and the National Tsing Hua University, Taiwan (102N2729E1 and Boost Program 99N2905E1). The authors would also like to thank Shin-Cheh Chen and Yi-Hong Chou for their clinical insights, which motivated this study, and appreciate James C. Wang's close reading of the manuscript.

References

1. American College of Radiology, *Breast Imaging Reporting and Data System, BI-RADS®—Mammography*, 3rd ed., American College of Radiology, Reston, VA (1998).
2. W. L. Teh et al., "Ultrasound guided core biopsy of suspicious mammographic calcifications using high frequency and power Doppler ultrasound," *Clin. Radiol.* **55**(5), 390–394 (2000).
3. S. A. Ermilov et al., "Laser optoacoustic imaging system for detection of breast cancer," *J. Biomed. Opt.* **14**(2), 024007 (2009).
4. M. Heijblom et al., "Visualizing breast cancer using the Twente photoacoustic mammoscope: what do we learn from twelve new patient measurements?," *Opt. Express* **20**(11), 11582–11597 (2012).
5. T.-C. Hsiao et al., "Visualization of microcalcifications using photoacoustic imaging: feasibility study," *Proc. SPIE* **7899**, 78992U (2011).
6. M. P. Morgan, M. M. Cooke, and G. M. McCarthy, "Microcalcifications associated with breast cancer: an epiphenomenon or biologically significant feature of selected tumors?," *J. Mammary Gland Biol. Neoplasia* **10**(2), 181–187 (2005).
7. J. Kang et al., "Optimal laser wavelength for photoacoustic imaging of breast microcalcifications," *Appl. Phys. Lett.* **99**(15), 153702 (2011).
8. K. Song and L. V. Wang, "Deep reflection-mode photoacoustic imaging of biological tissue," *J. Biomed. Opt.* **12**(6), 060503 (2007).
9. S. S. Buchbinder et al., "Can the size of microcalcifications predict malignancy of clusters at mammography?," *Acad. Radiol.* **9**(1), 18–25 (2002).
10. P.-C. Li and M.-L. Li, "Adaptive imaging using the generalized coherent factor," *IEEE Trans. Ultrason. Ferroelectr. Freq. Control* **50**(2), 128–141 (2003).
11. S. A. Pahl, M. J. C. van Gemert, and A. J. Welch, "Determining the optical properties of turbid media by using the adding-doubling method," *Appl. Opt.* **32**(4), 559–568 (1993).
12. S. Parker, "Laser-tissue interaction," *Br. Dent. J.* **202**(2), 73–81 (2007).
13. G. J. Cheng and C. Ye, "Experiment, thermal simulation, and characterizations on transmission laser coating of hydroxyapatite on metal implant," *J. Biomed. Mater. Res. A* **92**(1), 70–79 (2010).
14. E. C. Cho et al., "Measuring the optical absorption cross-sections of Au-Ag nanocages and Au nanorods by photoacoustic imaging," *J. Phys. Chem. C* **113**(21), 9023–9028 (2009).
15. P. Taroni et al., "In vivo absorption and scattering spectroscopy of biological tissues," *Photochem. Photobiol. Sci.* **2**(2), 124–129 (2003).
16. P. D. Tyr us and C. Diederich, "Two-dimensional acoustic attenuation mapping of high-temperature interstitial ultrasound lesions," *Phys. Med. Biol.* **49**(4), 533–546 (2004).
17. T. J. Allen and P. C. Beard, "Optimising the detection parameters for deep tissue photoacoustic imaging," *Proc. SPIE* **8223**, 82230 (2012).
18. J. R. Cleverley, A. R. Jackson, and A. C. Bateman, "Pre-operative localization of breast microcalcification using high-frequency ultrasound," *Clin. Radiol.* **52**(12), 924–926 (1997).
19. T. Li and R. J. Dewhurst, "Photoacoustic imaging in both soft and hard biological tissue," *J. Phys. Conf. Ser.* **214**, 012028 (2010).
20. R. E. Lenkinski et al., "Near-infrared fluorescence imaging of microcalcification in an animal model of breast cancer," *Acad. Radiol.* **10**(10), 1159–1164 (2003).
21. A. R. Cowen et al., "Visibility of microcalcifications in computed and screen-film mammography," *Phys. Med. Biol.* **42**(8), 1533–1548 (1997).